IEEE Access
Multidisciplinary | Rapid Review | Open Access Journal

Received 1 August 2023, accepted 24 August 2023, date of publication 28 August 2023, date of current version 5 September 2023.

Digital Object Identifier 10.1109/ACCESS.2023.3309556

RESEARCH ARTICLE

A Miniaturized Two-Element Antenna Array With High Isolation by Using Hybrid Electromagnetic Decoupling

MING YANG[1] AND JINZHI ZHOU[2]
[1]School of Electronics and Information Engineering, West Anhui University, Lu'an 237012, China
[2]Department of Electronics and Information Engineering, Bozhou University, Bozhou 236800, China

Corresponding author: Ming Yang (myang@ahu.edu.cn)

This work was supported in part by the Cultivation Funding Project of Excellent Top-Notch Talent of Colleges and Universities in Anhui Province under Grant gxgnfx2020118, in part by the Key Project of Natural Science Research of Colleges and Universities in Anhui Province under Grant KJ2020A0768, and in part by the Funding Project of Scientific Research Starting for the High-Level Talents of West Anhui University under Grant WGKQ2022009.

ABSTRACT A novel decoupling method combining magnetic coupling and electric coupling is proposed in this paper to design a miniaturized two-element antenna array. Different from the traditional planar decoupling structure, a three-dimensional quasi-split resonant ring decoupling structure which can realize electric coupling is introduced. The quasi-split resonant ring is composed of two meandered antenna elements printed on the top and bottom of the substrate. The other decoupling structure is composed of two parasitic patches, which realize magnetic coupling with the open end of the dipole element in the opposite plane. By properly controlling the strength of magnetic coupling and electric coupling, the induced currents can cancel each other out, thereby enhancing the isolation between adjacent ports. Compared with the antenna array employing the planar decoupling method, the size of the antenna array in this paper is significantly reduced by half. In terms of *S*-parameter and near-field radiation, the simulated results of the full-wave analysis are compared with the measured results. Essentially identical results successfully verify that the antenna achieves an isolation up to 27.5 dB and omnidirectional radiation mode in the resonant bandwidth of 1.76-1.80 GHz.

INDEX TERMS Antenna array, magnetic coupling, electric coupling, decoupling structure, parasitic patch, near-field.

I. INTRODUCTION

With the rapid development of wireless communication, wireless terminal put forward more stringent requirements for antenna miniaturization, easy integration, high isolation and high radiation efficiency, especially for multi-antenna systems [1], [2], [3], [4]. Multi-antenna system allows multiple antennas to be periodically distributed at intervals of half wavelength. The miniaturization of multi-antenna system can be achieved by reducing the antenna spacing, but the current distribution of antenna elements is also changed, which leads to the deterioration of impedance matching and radiation performance. Especially for the massive antenna system, the proper antenna-to-antenna spacing can effectively reduce the volume of the whole antenna system, which has been the research focus of multi-antenna system.

The latest literature reveals that many scholars have come up with novel ideas to solve the thorny problem of unexpected mutual coupling. Such as, metasurface, neutralization line, parallel coupled line, shorting via and decoupling network are successively applied to two-element and four-element antenna arrays, achieving excellent decoupling characteristics. In [5], a compact four-element antenna with better isolation than 30 dB is designed by combining the technology of neutralization line with two feeding network consisting of 180° phase shifter. In [6], a hybrid decoupling structure

The associate editor coordinating the review of this manuscript and approving it for publication was Tutku Karacolak.

is embedded in the common ground of the two antenna elements to achieve the purpose of decoupling. By adjusting the dimension of decoupling branch reasonably, a lumped parallel *LC* resonator with optimal equivalent inductance and capacitance is obtained. Benefited to the equivalent *LC* resonator, the isolation in multiple frequency points are enhanced. However, the decoupled structure composed of parasitic U-shaped slot and lumped capacitance increases the complexity of antenna design. In [7], 10 pairs of L-shaped slots are etched on the metallic sheet as an integrated, quarter-wavelength sleeve choke or bazooka balun to suppress the surface current on the outer conductor of coaxial cable [8]. Lumped capacitors are also loaded to miniaturize the entire size. A metasurface with a negative permeability is employed above a two-element antenna array in [9] to improve the port isolation. Electromagnetic band-gap (EBG) with cross-slot is introduced in [10] to suppress the mutual coupling between two patch antennas. Attribute to the stop-band characteristics of the fractal EBG, an average coupling suppression of 18 dB is obtained in the measurements. In [11], a hybrid decoupling structure composed of neutralization dielectric substrate and metal baffle, which is applied to design base station arrays. A neutralization dielectric substrate based on the neutralization theory provides a new signal path for reflected waves and cancels out the original mutual coupling. Metal baffle is utilized to suppress the propagation of electromagnetic waves in free space. Combining two decoupling structures, the measured results show that the isolation between any two ports in the four unit array is better than 20 dB. A novel decoupling strategy that integrated surrounding resonance net, array-antenna decoupling surface and composite decoupling surface are introduced to reduce concurrently multicoupling in [12]. The measured result show that the hybrid decoupling scheme has the advantage of isolation up to 25 dB, which is suitable for base station. Innovative feeding forms can also achieve high isolation characteristics. For example, [13] proposes to introduce hybrid feed design consisting of a balanced-probe feed and a slot-coupled feed based on stacked patch antennas to achieve 43 dB isolation between vertical and horizontal ports. Similarly, [14] designs a four-unit antenna with 40.6 dB port isolation by combining quadrature feeding network and multilayer printed circuit board (PCB) technology.

In the latest publications, simpler and more innovative approaches are proposed to reduce the coupling between multiple ports. Such as, in [15], a pair of parallel coupled line resonators (PCR) composed of six coupled lines are placed between two-element antenna arrays. Attribute to the band reject characteristic of PCR, the isolation of the antenna array is improved to 26.2 dB. Furthermore, the antenna gain and radiation efficiency are also improved. Different from [15], two groups of parallel shorting vias are inserted into the non-radiating edges of two patches to balance the mutual capacitive and inductive couplings. Then the feature of high isolation within broadband is obtained in [16]. In [17], a linear antenna array is proposed by placing the patch antenna and the monopole antenna at intervals. Attributes to the periodic distribution, the mutual coupling between non-adjacent patch antennas cancels the coupling between the patch antennas and the adjacent dipole antennas.

The decoupling theory mentioned above is applied on the basis of planar array antenna, whether introducing decoupling structure or stimulates multiple decoupling modes. So the more antenna elements there are, the larger the area occupied by the array. In this paper, a novel decoupling theory is proposed, which not only generates the decoupling effect but also reduces the size of the antenna array by half. Two C-shaped dipole antennas are printed on the upper and lower surfaces of substrate respectively to form a three-dimensional two-element antenna array with mutual electric coupling. Two parasitic patches are further introduced to stimulate magnetic coupling with the antenna array. When the mutual magnetic coupling and mutual electric coupling are properly combined, the coupling currents cancel each other out, improving the port isolation of the miniaturized antenna array.

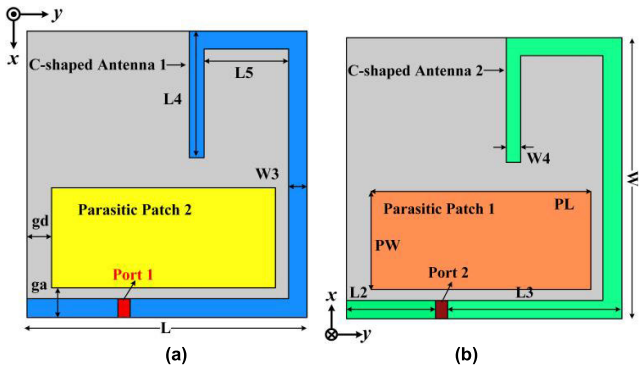

FIGURE 1. Geometry of the designed miniaturized two-element patch antenna array: (a) top view of substrate; (b) bottom view of substrate. L = 22.5, L2 = 7.3, L3 = 14.2, L4 = 10.2, L5 = 6.75, W = 23, W3 = 1.5, W4 = 1.2, PL = 18, PW = 8, ga = 2.4; gd = 2 (all dimensions in mm).

II. ANTENNA ARRAY DESIGN AND DECOUPLING ANALYSIS

Fig. 1 shows the structure diagram of the proposed miniaturized two-element antenna array. The antenna array consists of two dipole antenna elements with the same structure. Different from the conventional dipole, the radiation part of the dipole designed in this paper is bent into C-shape to offset the unexpected coupling currents. Two C-shaped dipole patches are printed centrosymmetrically on the upper and lower surface of the FR4 substrate with relative permittivity of 4.4 and a height of 0.8 mm. Meanwhile, two rectangular parasitic patches are symmetrically placed on the upper and lower surfaces of the substrate, which are employed for magnetic coupling with the open end of the C-shaped dipole and weaken the coupling current on the excitation port.

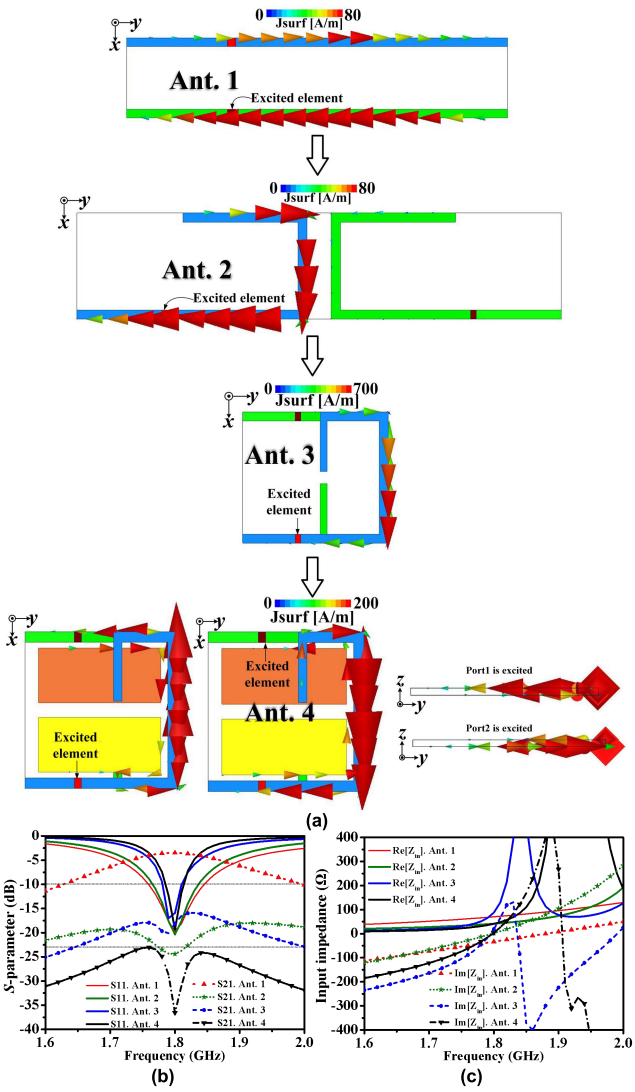

FIGURE 2. The evolution of the miniaturized high isolation antenna and simulated result of the corresponding antenna. (a) antenna evolution; (b) simulated result of S-parameter; (c) simulated result of input impedance.

A. MECHANISM OF HIGH ISOLATION AND MINIATURIZATION OF C-SHAPED DIPOLE ANTENNA

In order to explain the theory of miniaturization and high isolation more clearly. Fig. 2 shows the evolution process of antenna and the simulated *S*-parameters of the corresponding antenna. Firstly, a traditional two-element dipole antenna array with a parallel structure is proposed and named as Ant. 1 in Fig. 2(a). The simulated *S*-parameters show that the S_{11} of Ant. 1 meets the requirement of $\leq$ -10 dB in the range of 1.76-1.84 GHz. However, the isolation between the two ports is only 4 dB, which is mainly related to the placement of the two dipoles, physical dimensions and the properties of the coupling currents, such as the strong coupling currents of adjacent ports in Fig. 2(a). Ant. 2 is based on Ant. 1 by meandering the radiating part. Since the dipole sizes of Ant. 1 and Ant. 2 do not change, the two antennas have substantially the same resonant characteristics. The change in the position of the feeding point only make the impedance matching of the two antennas slightly different. Moreover, due to the meandering technique, both the parallel coupling mode and the collinear coupling mode are acquired in Ant. 2. The intensity and phase of the coupling current can be changed by adjusting the length of the bent branch properly. Appropriate phase and current intensity can produce partial current cancellation effect as shown in Fig. 2(a). Then, Ant. 2 in Fig. 2(b) achieve high isolation characteristic of 24 dB at 1.8 GHz. Based on the planar distribution of Ant. 2, Ant. 3 with the three-dimensional distribution architecture is adopted. The dimension of Ant. 3 is obviously reduced by half. However, Fig. 2(b) reveals that the isolation of Ant. 3 is reduced by more than 5 dB compared to Ant. 2, which is mainly due to the vertically symmetrical placement of the two dipole elements, forcing current coupling to adjacent ports. The current profile of Ant. 3 depicted in Fig. 2(a) further explains the deterioration in isolation. During the evolution from Ant. 2 to Ant. 3, the resonant bandwidth of the antenna decreased from 3.33% (1.77-1.83GHz) to 1.67% (1.78-1.81GHz). The reason for this bandwidth reduction is due to the effect of current crowding associated with junction discontinuities introduced by the application of meandering. In other words, near the bends, the current spikes and the phenomenon of steep impedance change caused by this effect can be clearly observed in Fig. 2(c). In order to further improve the port isolation on the basis of miniaturization, two rectangular parasitic patches are printed on the upper and lower surfaces of the array. Finally, Ant. 4 with isolation as high as 36.5 dB at 1.8 GHz is designed, as shown in Fig. 2(a).

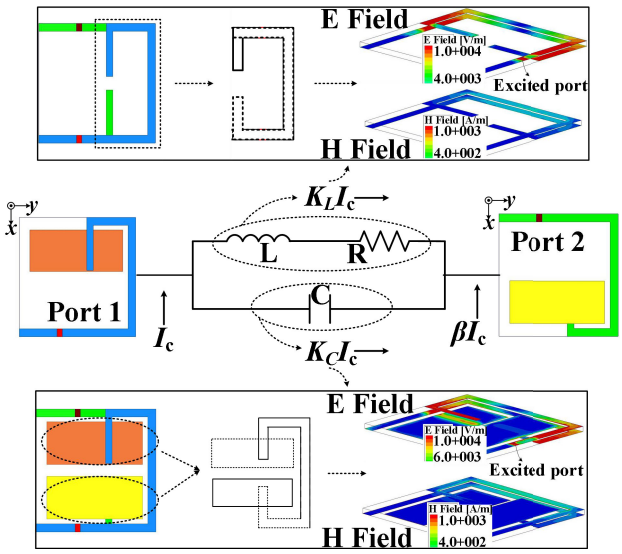

FIGURE 3. Equivalent model of the hybrid electromagnetic decoupling.

Equivalent circuit model of the hybrid electromagnetic decoupling is given in Fig. 3 to explain the decoupling mechanism of Ant. 4. As shown in Fig. 3, when port 1 is excited

by current I_c, the coupling current on port 2 is βI_c. When the two C-shaped dipoles are placed symmetrically up and down, two C-shaped dipole antennas together form a quasi-split resonant ring (QSRR). Then the induced current $K_L I_c$ is introduced due to the electric coupling effect of QSRR. In addition, two rectangular parasitic patches distributed on the upper and lower layers are magnetically coupled with the open end of C-shaped dipole, respectively, to generate an induced current $K_C I_c$. On purpose to improve the isolation between two ports, only the size of parasitic patch and the length of open end of dipole need to be properly adjusted so that the three induced currents meet the following requirements:

$$\beta I_c + K_L I_c + K_C I_c = 0 \tag{1}$$

$$\frac{K_L}{K_C} = \frac{1/j\omega C}{j\omega L + R} \tag{2}$$

The parasitic patches combined with QSRR can be modeled as an inductance L with an internal resistance R and a capacitance C in parallel, which correspond to the magnetic and electric coupling, respectively. Combined magnetic coupling and electric coupling, the unexpected coupling current cancels each other to achieve decoupling effect. Eq. (2) indicates that the strength of magnetic coupling and electric coupling can be further optimized by adjusting the capacitance C and inductance L. In other words, increasing the size of the QSRR is beneficial to improve the electrical coupling strength, and changing the distance between the parasitic patch and the dipole can also improve the magnetic coupling strength. It is precisely by adhering to this design guideline that the two decoupling methods are flexibly adjusted.

In order to further elucidate the role of QSRR and the parasitic patch in decoupling, a series of parameter analyses are performed. The specific simulated results are presented at Fig. 4 and Fig. 5. It can be seen from Fig. 4(a) and Fig. 4(c) that although ga has little effect on the resonance characteristics, the port isolation in the resonant bandwidth changes significantly. In other words, the reflection coefficient and port isolation at 1.8 GHz deteriorate considerably when the parasitic patch is moved close to or far from the dipole to a certain extent. According to the simulated results, it is better to choose the optimal ga in the range of 2.1-2.7 mm. With the increase of PL and L4, the resonant frequency of the antenna gradually shifts to low frequency. Although the isolation between the two ports is basically unchanged at the beginning, as PL and L4 continue to increase above 18 mm and 10.2 mm respectively, the decoupling effect at the resonant frequency gradually weakens. Fig. 4(d) also shows the curve of S-parameter changing with the length of C-shaped. Intuitively, with increase of L5, the total length of dipole antenna gradually increases, which directly causes the resonant frequency to shift to lower frequencies, which is similar to L4. The relationship between L5 and port isolation is similar to that of ga, which is not discussed here for brevity.

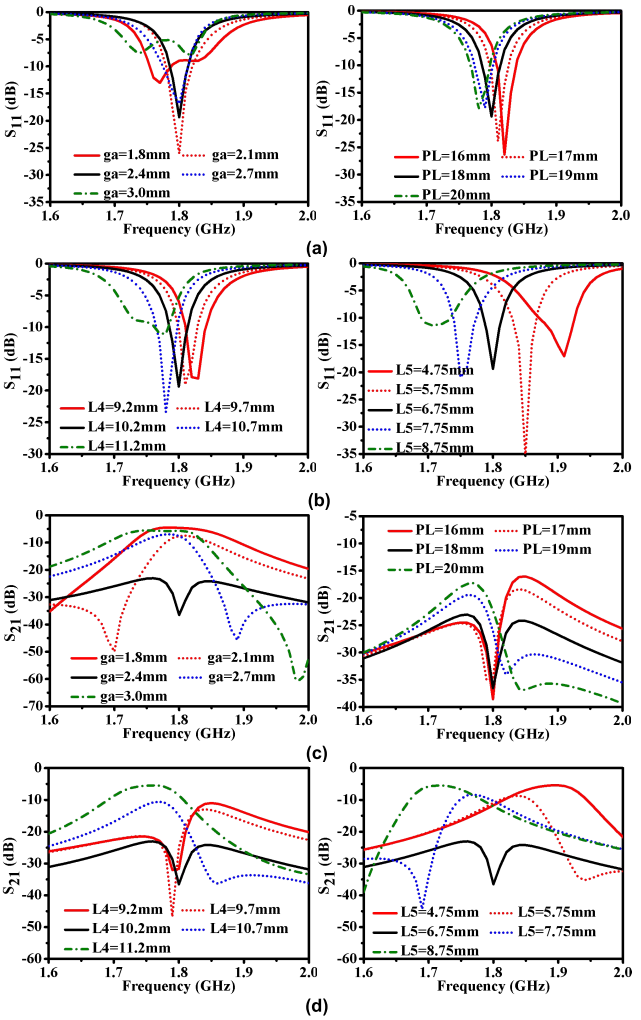

FIGURE 4. The effect of different parameters on simulated S-parameter of Ant. 4. (a) different ga and PL on S11; (b) different L4 and L5 on S11; (c) different ga and PL on S21; (d) different L4 and L5 on S21.

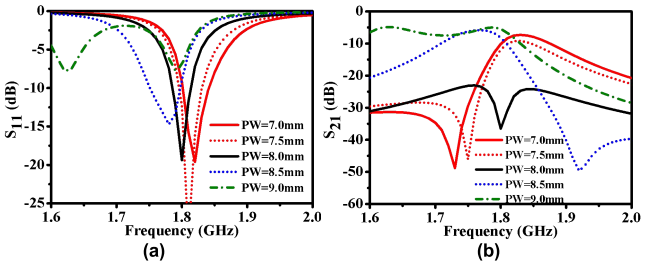

FIGURE 5. The effect of different PW on simulated S-parameter of Ant. 4. (a) different PW on S11; (b) different PW on S21.

The following Fig. 5 shows the curve of S-parameters of Ant. 4 variation with the width of parasitic patch. It can be seen from the Fig. 5(a) that as the width of the parasitic patch PW increases from 7 mm to 9 mm, the resonant point of the antenna gradually moves to the low frequency. On the contrary, with the increase of PW, the frequency point where the optimal antenna isolation is located gradually moves to

high frequency. Therefore, the problem that the resonance frequency point of the antenna is not at the same frequency point as the optimal isolation can be effectively solved by adjusting PW.

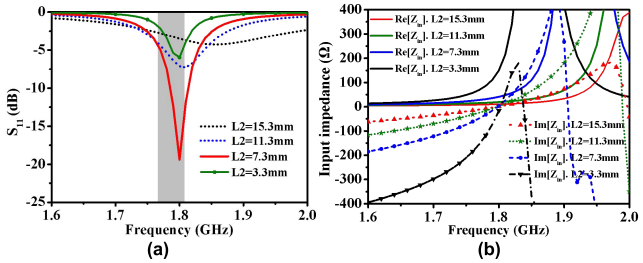

FIGURE 6. The effect of different L2 on simulated S11 and input impedance of Ant. 4. (a) different L2 on S11; (b) different L2 on input impedance.

Fig. 6 shows the curves of the reflection coefficient and input impedance of the Ant. 4 changing with frequency when L2 takes different values. It should be pointed out that L2 represents the distance from the feed point to the left open-end of the dipole as depicted in Fig. 1(b). As L2 decreases, it means that the feed point gradually moves from the center to the left open-end. As shown in Fig. 6(b), as L2 gradually decreases from 15.3 mm to 3.3 mm, the real part of the input impedance at the resonance point gradually increases from $< 50\ \Omega$ to infinity while the imaginary part remains unchanged. In consequence, an optimal feed position must exist in between the center-point and open-end where the input impedance is equal to 50 Ω. In other words, there are two such impedance matched positions (one for each open-end) for meandered half wavelength dipole. It is worth noting that the parameter analysis results in Fig. 6 are the same as the results in [18], [19], [20], and [21].

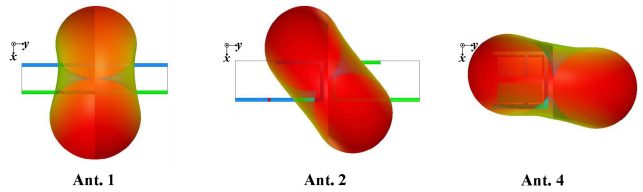

FIGURE 7. Simulated 3-D radiation pattern of three antennas. (Ant. 1, Ant. 2 and Ant. 4.)

B. POLARIZATION AND RADIATION FIELD OF C-SHAPED DIPOLE ANTENNA

In order to explain the influence of bending effect on polarization and radiation field, simulated radiation patterns of the dipole antennas (Ant. 1, Ant. 2 and Ant. 4) are presented at Fig. 7 and Fig. 8. In these plots, the radiated power density is decomposed into two orthogonal polarization components (G_{phi} and G_{theta}). For straight dipole (Ant. 1), the current flows along the y-direction only (Fig. 2).

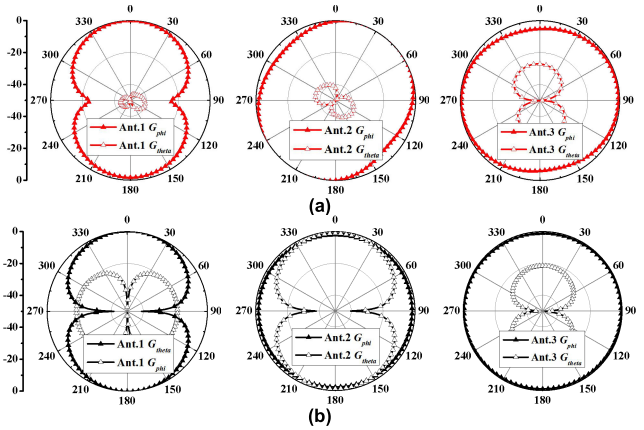

FIGURE 8. Simulated radiation pattern of three antennas (Ant. 1, Ant. 2 and Ant. 4) in xoy and yoz-planes. (a) xoy-plane; (b) yoz-plane.

Referring to Fig. 8(a) and 8(b), G_{phi} is the main polarization and directional pattern is observed (xoy-plane). On yoz-plane, G_{theta} dominates with directional pattern. Both cross polarization levels (G_{theta} on xoy-plane and G_{phi} on yoz-plane) are found to be small (suppression $>$ 30 dB). With Ant. 2 meandering, current is forced to flow along both x and y directions. On the xoy-plane, due to the bending effect of the Ant. 2, two currents flowing in opposite directions along the y axis, and the radiation brought by partial currents in the far field cancels each other out. After cancellation, the remaining current along the y axis and the current along the x axis are superimposed in the far field to form a radiation pattern with the main beam along the direction of phi $=$ 45° (Fig. 7 and Fig. 8(a)). While, the currents in the x and y directions are the main contribution of G_{theta} and G_{phi} respectively on yoz-plane. With reference to Fig. 8(b), these decomposed radiation components (G_{theta} and G_{phi}) are comparable in strength. When Ant. 4 meandering is introduced, current will also flow along x and y directions. On the xoy-plane, more current flows along the x-axis, so the main beam of the radiation pattern is nearly parallel to the y-axis (Fig. 7 and Fig. 8(a)). Due to the different current densities and directions along the x-axis and y-axis, the intensity of G_{phi} on the yoz-plane is higher than that of G_{theta}. Then the omnidirectional radiation characteristics in the yoz- plane is obtained.

As analyzed above, the Ant. 4 decoupled by magnetic coupling and electric coupling exhibits excellent characteristics, making it stand out in the evolution of antennas. The measurements of the Ant. 4 and the comparison with published antennas will be highlighted in the next chapter.

III. MEASURED RESULTS DISCUSSION AND COMPARISON

A photograph of the fabricated miniaturized antenna is given in Fig. 9(a). In order to verify the decoupling features and radiation characteristics of the two-port antenna system, test items related to reflection coefficient, antenna gain, radiation

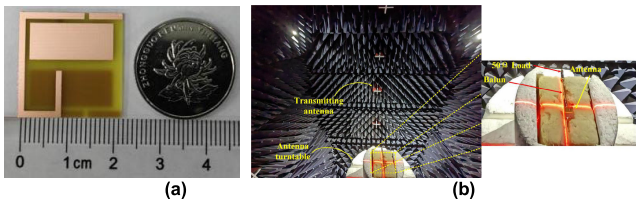

FIGURE 9. (a) Photography of the fabricated miniaturized two-element patch antenna array; (b) test scenario.

efficiency and radiation pattern are carried out successively. Among them, the vector network analyzer *ZNB8* of *Rod Schwartz* is utilized to test *S*-parameter, and other indexes are carried out in the chamber of *General Test* shown in Fig. 9(b).

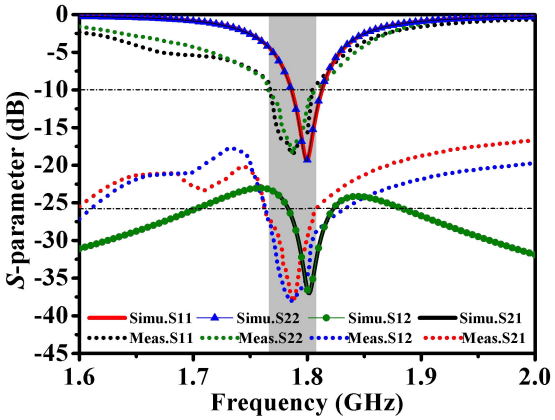

FIGURE 10. Comparison curve between simulated results and measured results of S-parameter.

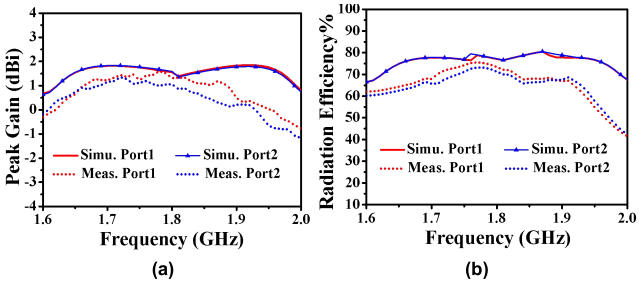

FIGURE 11. Simulated and measured gains and radiation efficiencies of the designed antenna. (a) peak gain; (b) radiation efficiency.

The simulated results and measured results of *S*-parameter are presented at Fig. 10 for comparison. The measured resonance point is 1.78 GHz, shifting to the low frequency by 20 MHz. Meanwhile, the measured port isolation up to 38 dB also verifies that the effect of joint decoupling plays a key role. Fig. 11(a) shows the curve of peak gain with frequency. The simulated results are basically consistent with the measured results. The maximum gain over the resonance bandwidth is 1.27 dBi, which is 0.34 dB below than the maximum simulated gain of 1.61 dBi. The comparison of radiation efficiency is shown in Fig. 11(b). It can be seen that the radiation efficiency of two ports has the same variation trend with frequency. The measured radiation efficiency is best at 1.77 GHz, where the radiation efficiency of port 1 is 75.5% and that of port 2 is 73.2%. Compared with the simulated results, the radiation efficiency decreased by 4.6%. It should be mentioned that the deviation between the simulated results and the measured results is mainly caused by the errors in the manufacturing, testing and welding.

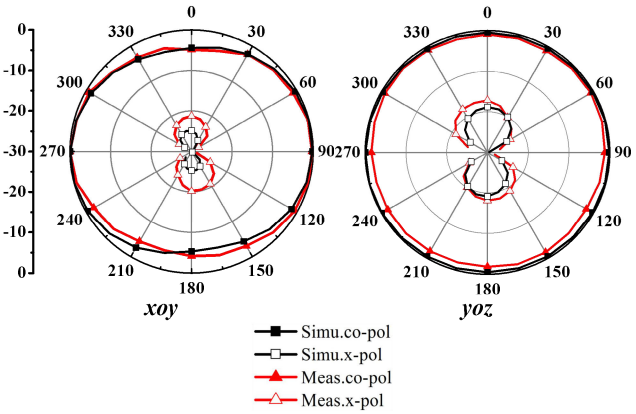

FIGURE 12. Simulated and measured radiation patterns of the designed antenna in xoy and yoz-planes at 1.78 GHz.

As for the radiation pattern, the simulated results and measured results of 1.78 GHz in *xoy*-plane and *yoz*-plane are given in Fig. 12 when port 1 is excited. It is worth noting that when the test port is excited, the other port needs to be terminated by 50 Ω load. It can be obtained from Fig. 12 that the designed antenna shows omnidirectional radiation characteristics, which is the same as the simulated results.

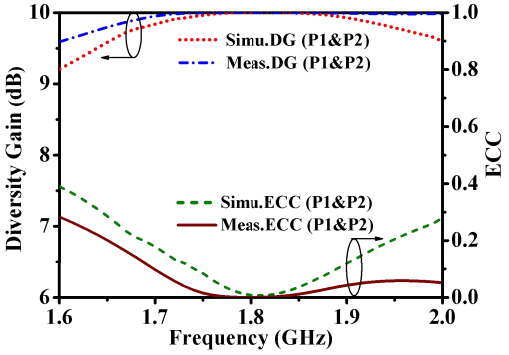

FIGURE 13. Comparison chart of simulated results and measured results of ECC and DG.

Meanwhile, the envelope correlation coefficient (ECC) shown in Fig. 13 is calculated by the following formula (3). Among them, $E_i(\theta, \varphi)$ represents 3-D radiation pattern for

$$\left|\rho_{ij}^{s}\right|^2 = \rho_{eij}^{s} = \frac{\left|\iint_{4\pi}\left[E_i(\theta,\varphi) * E_j(\theta,\varphi)\right] d\Omega\right|^2}{\iint_{4\pi}\left|E_i(\theta,\varphi)^2\right| d\Omega \iint_{4\pi}\left|E_j(\theta,\varphi)^2\right| d\Omega} \tag{3}$$

$$DG = 10 \times \sqrt{1 - \left|\rho_{eij}^{s}\right|} \tag{4}$$

antenna *i* [22], [23]. It can be concluded from Fig. 13 that the measured ECC meets the requirement of less than 0.1 within the antenna resonance frequency band. At the same time, the diversity gain (DG) calculated by formula (4) also approximately meets the requirement of 10 dB.

TABLE 1. Comparison results with published antennas.

Ref	RFP (GHz)	Effi (%)	Isolation (dB)	Size (λ_0^3)	NAE	ES (λ_0)
[1]	2.45	≥ 75	10~20	0.47×0.18×0.007	2	0.04
[3]	1.511	≥ 83	≥ 26	π×0.09×0.049	2	0.5
[5]	0.925 1.95	-	≥ 30	0.31×0.19×0.006	4	0.19
[9]	5.8	≥ 65	≥ 20	0.77×0.5×0.12	2	0.02
[10]	5.05	-	≥ 33	0.5×0.8×0.03	2	0.22
[11]	1.95	≥ 89	≥ 20	0.38×0.75×0.42	16	0.38
[14]	2.45	≥ 40	≥ 40.8	1×1×0.03	4	0.5
[15]	3.5	≥ 80	≥ 26	0.76×0.58×0.019	2	0.07
[16]	3.555	≥ 72	≥ 27	0.26×0.66×0.1	2	0.005
[17]	3.5	≥ 80	≥ 20	2.68×1.17×0.165	4	0.467
This work	**1.783**	**≥ 70**	**≥ 27.5**	**0.13×0.13×0.005**	**2**	**0.005**

RFP represents resonance frequency point; λ_0 represents the wavelength of the center frequency in free space; NAE represents number of antenna elements; ES represents element separation.

A detailed comparison with published antennas in terms of resonant frequency point, radiation efficiency, antenna size and port isolation is shown in Table 1. Among them, the high isolation brought by the decoupling method proposed in [1], [9], [11], and [17] is slightly inferior to 27.5 dB in this paper. In [3], [5], [10], [14], [15], and [16], perfect isolation and high radiation efficiency are obtained. However, the multi-layer structure up to four layers, additional power division network and traditional planar decoupling form on the one hand increase the difficulty of antenna design and processing cost on the one hand. On the other hand, it is not conducive to the miniaturization of antenna array. Compared with this paper, the isolation between ports is enhanced by the combination of upper and lower decoupled branches in a single-layer structure. Furthermore, the purpose of miniaturization is also achieved. Overall, the design in this paper is simple, low cost, and easy to manufacture.

IV. CONCLUSION

A miniaturized two-element antenna array with high isolation is firstly investigated in this paper by employing the technology of hybrid electromagnetic decoupling. The edge-to-edge distance between the two dipole antennas is only $0.005\lambda_0$. The measured results consistent with the simulated results show that the decoupling effect better than 27.5 dB, the gain of 1.27 dBi and the radiation efficiency of 73.2% are achieved in the frequency range of 1.76-1.80 GHz. More importantly, the volume of antenna array is effectively reduced by 50%. The miniaturization and isolation enhancement methods proposed in this paper can be extended to other frequency bands, mainly by adjusting the length of bent dipoles and the size of parasitic patches. Therefore, extending plane decoupling to three-dimensional decoupling provides a new idea for improving the isolation of antenna array and system miniaturization in handheld radio systems and wearable applications.

REFERENCES

[1] S.-C. Chen, Y.-S. Wang, and S.-J. Chung, "A decoupling technique for increasing the port isolation between two strongly coupled antennas," *IEEE Trans. Antennas Propag.*, vol. 56, no. 12, pp. 3650–3658, Dec. 2008.

[2] Y. Li, C.-Y.-D. Sim, Y. Luo, and G. Yang, "High-isolation 3.5 GHz eight-antenna MIMO array using balanced open-slot antenna element for 5G smartphones," *IEEE Trans. Antennas Propag.*, vol. 67, no. 6, pp. 3820–3830, Jun. 2019.

[3] M.-C. Tang, X. Chen, T. Shi, H. Tu, Z. Wu, and R. W. Ziolkowski, "A compact, low-profile, broadside radiating two-element Huygens dipole array facilitated by a custom-designed decoupling element," *IEEE Trans. Antennas Propag.*, vol. 69, no. 8, pp. 4546–4557, Aug. 2021.

[4] Y. Xiao, Y. Qi, W. Yu, Y.-H. Bi, X. Su, C. Wu, Q. Liu, and J. Fan, "A planar low-profile meander antenna design for wireless terminal achieving low RF interference and high isolation in multi-antenna systems," *IEEE Trans. Electromagn. Compat.*, vol. 64, no. 3, pp. 674–682, Jun. 2022.

[5] H.-L. Peng, R. Tao, W.-Y. Yin, and J.-F. Mao, "A novel compact dual-band antenna array with high isolations realized using the neutralization technique," *IEEE Trans. Antennas Propag.*, vol. 61, no. 4, pp. 1956–1962, Apr. 2013.

[6] Q. Sun, B. Sun, L. Sun, W. Huang, and Q. Ren, "Broadband two-element array with hybrid decoupling structures for multimode mobile terminals," *IEEE Antennas Wireless Propag. Lett.*, vol. 14, pp. 1431–1434, 2015.

[7] X. Yang, B. Sun, L. Sun, J. Guo, and Y. Zou, "Broadband and miniaturized structure loaded with lumped capacitors for parasitic current reduction," *IEEE Antennas Wireless Propag. Lett.*, vol. 11, pp. 1010–1013, 2012.

[8] S.-W. Su and T.-C. Hong, "Radiation improvement of printed, shorted monopole antenna for USB dongle by integrating choke sleeves on the system ground," *IEEE Trans. Antennas Propag.*, vol. 59, no. 11, pp. 4383–4388, Nov. 2011.

[9] Z. Wang, C. Li, and Y. Yin, "A meta-surface antenna array decoupling (MAAD) design to improve the isolation performance in a MIMO system," *IEEE Access*, vol. 8, pp. 61797–61805, 2020.

[10] X. Yang, Y. Liu, Y.-X. Xu, and S.-X. Gong, "Isolation enhancement in patch antenna array with fractal UC-EBG structure and cross slot," *IEEE Antennas Wireless Propag. Lett.*, vol. 16, pp. 2175–2178, 2017.

[11] B. Liu, Y. Da, X. Chen, and A. A. Kishk, "Hybrid decoupling structure based on neutralization and partition schemes for compact large-scale base station arrays," *IEEE Antennas Wireless Propag. Lett.*, vol. 21, no. 2, pp. 267–271, Feb. 2022.

[12] J. Li, H. Zhai, L. Zhao, T. Chen, Y. Wang, S. Yang, and W. Xu, "High-capacity compact massive MIMO array with hybrid decoupling scheme," *IEEE Trans. Antennas Propag.*, vol. 70, no. 10, pp. 9292–9304, Oct. 2022.

[13] H. Saeidi-Manesh and G. Zhang, "High-isolation, low cross-polarization, dual-polarization, hybrid feed microstrip patch array antenna for MPAR application," *IEEE Trans. Antennas Propag.*, vol. 66, no. 5, pp. 2326–2332, May 2018.

[14] D. Wu, Y.-X. Sun, B. Wang, and R. Lian, "A compact, monostatic, co-circularly polarized simultaneous transmit and receive (STAR) antenna with high isolation," *IEEE Antennas Wireless Propag. Lett.*, vol. 19, no. 7, pp. 1127–1131, Jul. 2020.

[15] K. S. Vishvaksenan, K. Mithra, R. Kalaiarasan, and K. S. Raj, "Mutual coupling reduction in microstrip patch antenna arrays using parallel coupled-line resonators," *IEEE Antennas Wireless Propag. Lett.*, vol. 16, pp. 2146–2149, 2017.
[16] R. Zaker and A. Kheirdoost, "Bandwidth and isolation improvement of highly coupled printed array antenna using multiple shorting posts," *IEEE Trans. Antennas Propag.*, vol. 69, no. 11, pp. 7987–7992, Nov. 2021.
[17] Y.-F. Cheng, J. Liu, C. Wei, W.-J. Wu, L. Sun, and G. Wang, "Interplanted patch-monopole array with enhanced isolation," *IEEE Antennas Wireless Propag. Lett.*, vol. 21, no. 8, pp. 1664–1668, Aug. 2022.
[18] C. Song, Y. Huang, J. Zhou, P. Carter, S. Yuan, Q. Xu, and Z. Fei, "Matching network elimination in broadband rectennas for high-efficiency wireless power transfer and energy harvesting," *IEEE Trans. Ind. Electron.*, vol. 64, no. 5, pp. 3950–3961, May 2017.
[19] R. King, "Asymmetrically driven antennas and the sleeve dipole," *Proc. IRE*, vol. 38, no. 10, pp. 1154–1164, Oct. 1950.
[20] R. King and T. Wu, "The cylindrical antenna with arbitrary driving point," *IEEE Trans. Antennas Propag.*, vol. AP-13, no. 5, pp. 710–718, Sep. 1965.
[21] H. Chu, Y.-X. Guo, and Z. Wang, "60-GHz LTCC wideband vertical off-center dipole antenna and arrays," *IEEE Trans. Antennas Propag.*, vol. 61, no. 1, pp. 153–161, Jan. 2013.
[22] M. S. Sharawi, "Current misuses and future prospects for printed multiple-input, multiple-output antenna systems [wireless corner]," *IEEE Antennas Propag. Mag.*, vol. 59, no. 2, pp. 162–170, Apr. 2017.
[23] M. Ameen, O. Ahmad, and R. K. Chaudhary, "Bandwidth and gain enhancement of triple-band MIMO antenna incorporating metasurface-based reflector for WLAN/WiMAX applications," *IET Microw., Antennas Propag.*, vol. 14, no. 13, pp. 1493–1503, Oct. 2020.

MING YANG was born in 1982. He received the B.S. degree from Huaibei Normal University, in 2005, and the M.S. and Ph.D. degrees in electromagnetic field and microwave technology from Anhui University, Hefei, China, in 2010 and 2019, respectively.

He is currently the Deputy Director of the School of Electronics and Information Engineering, West Anhui University, Lu'an, China. He is the author and coauthor of about 20 scientific papers published in journals and presented at international conferences in the field of antenna design. His current research interests include MIMO antennas for hand-held devices, SIW antennas, base station antennas, multi-band antennas, millimeter wave antennas, and antenna array design.

JINZHI ZHOU was born in Suzhou, Anhui, China, in 1982. She received the M.S. degree in computer software and theory from Huaibei Normal University, in 2011.

Her current research interests include MIMO antennas, circularly polarized antennas, embedded system design, computational electromagnetics, and antenna theory and technology.